

Geometrically nonlinear analysis of FG doubly-curved and hyperbolical shells via laminated by new element

M. Rezaiee-Pajand^{*}, Amir R. Masoodi^a and E. Arabi^b

Departement of Civil Engineering, Ferdowsi University of Mashhad, Islamic Republic of Iran

(Received April 13, 2018, Revised May 24, 2018, Accepted June 2, 2018)

Abstract. An isoparametric six-node triangular element is utilized for geometrically nonlinear analysis of functionally graded (FG) shells. To overcome the shear and membrane locking, the element is improved by using strain interpolation functions. The Total Lagrangian formulation is employed to include the large displacements and rotations. Finding the nonlinear behavior of FG shells via laminated modeling is also the goal. A power function is employed to formulate the variation of elastic modulus through the thickness of shells. The results are presented in two ways, including the general FGM formulation and the laminated modeling. The equilibrium path is obtained by using the Generalized Displacement Control Method. Some popular benchmarks, including hyperbolical shell structures are solved to declare the correctness and accuracy of proposed formulations.

Keywords: geometrically nonlinear analysis; functionally graded materials (FGMs); laminate theory; degenerated six-node triangular element; Total Lagrangian formulation; hyperbolical shell

1. Introduction

In the past decades, some innovative computational methods have been developed for geometrically nonlinear analysis of shells. As a tool, several new shell elements were proposed by using various types of formulation. It is well established that the most important developments of shell structure analyses are based on the finite element method. According to the related literature, flat facet element, solid 3D element, degenerated shell element and 2D shell element based on the shell theory are the four types of finite element formulations used for these kinds of analyses. Among them, the last two methods are more applicable. The first motivation concerned the degenerated shell element theory was proposed by Ahmad *et al.* (1970) for analyzing the curved shell structures. After that, the researches of Hughes and Liu (1981a, b), Dvorkin and Bathe (1984), Park and Stanley (1986), and Liu *et al.* (1986) among the many other studies represented the same method for investigating the behavior of shell. Furthermore, the books of Bathe (1982) and Crisfield (1986), expressed the general subjects of the degenerated shell element procedure with some numerical examples.

In spite of the merits of using degenerated elements, such as, simpler formulation and less computational efforts, the lower-order elements within this group suffer from

locking phenomenon. Among the different methods proposed for alleviating locking problems, one can note the Mixed Interpolation of Tensorial Components (MITC). The MITC formulation was widely used to develop shell elements for linear and nonlinear analyses. In 2004, Lee and Bathe (2004) presented an isotropic triangular shell finite element based on this approach. In addition to these, a finite element computational model for the nonlinear analysis of shell structures was proposed by Arciniega and Reddy (2007). They used a family of higher-order elements with Lagrangian interpolations to avoid the shear and membrane locking. Recently, some other researches were performed about employing MITC formulation to develop triangular shell element for nonlinear analysis of shell-like structures under mechanical and thermal loads (Masoodi and Arabi 2018, Rezaiee-Pajand *et al.* (2018a).

Nowadays, the use of composite materials, due to their modified properties, is widely developed in different industries. Among them, functionally graded and composite laminated materials have received more attention. As a result, the interests of studying the behavior of functionally graded material (FGM) components have increased in the recent years. This is also due to their functional gradation and avoiding the material mismatch. The potential reduction of in-plane and transverse through-the-thickness stresses, an improved residual stress distribution, enhanced thermal properties, higher fracture toughness, and reduced stress intensity factors are some of the benefits of utilizing FGMs in structures. In these materials, the ceramic part provides high-temperature resistance due to its low thermal conductivity while the structural strength is established by the ductile metal part. Hence, this material can be also used to control the thermal deformation (Wetherhold *et al.* 1996). Using these materials in beam structures was widely investigated by researchers (Rezaiee-Pajand and Masoodi

*Corresponding author, Professor,
E-mail: rezaiee@um.ac.ir

^a Ph.D. Candidate,
E-mail: amirreza.masoodi@mail.um.ac.ir

^b Ph.D. Candidate,
E-mail: elias.arabi@mail.um.ac.ir

2018, Rezaiee-Pajand *et al.* 2018b) while it has not been performed adequate studies on the behavior of FG shell structures, especially based on the equivalent single layer theory.

Many researches were performed for various analyses of the FG shells. An analytical solution was presented for large deformation analysis of FG plates and shallow shells by Woo and Meguid (2001). The geometrically nonlinear analysis of FG shells was studied by Arciniega and Reddy (2007a). High-order Lagrangian interpolation functions were utilized to approximate the field variables to avoid membrane, shear, and thickness locking. Moreover, a four-node quasi-conforming shell element was developed by Kim *et al.* (2008) for geometrically nonlinear analysis of the FGM plates and shells. They concentrated on the effects of the volume fractions in the mechanical properties of FG plates and shells. In another research, Barbosa and Ferreira (2009) studied the geometrically nonlinear analysis of FG plates and shells using Margurre shell element. Furthermore, the geometrically nonlinear analysis of FG shells was performed by Zhao and Liew (2009). They used a modified version of Sander's nonlinear shell theory in which the von Karman strains used for geometric nonlinearity. Another research about the application of triangular element for geometrically nonlinear analysis of FG shells was incorporated by Levyakov and Kuznetsov (2011). In 2015, a review article was published about the theories for modeling and analysis of FG plates and shells by Thai and Kim (2015). Moreover, an enhanced assumed strain shell element was extended for nonlinear analysis of FG structures by Beheshti and Ramezani (2015). Recently, several researches were dedicated to buckling and nonlinear analysis of plates and shells made of isotropic FGMs including truncated conical and spherical shells (Kaci *et al.* 2014, Uysal 2016, Khayat *et al.* 2017).

On the other hand, increasing application of composite materials in engineering fields demands proper theories to take into account the effects of adopting these types of material on the behavior of structures, especially in the nonlinear analysis (Kapania 1989, Reddy and Arciniega 2004). In 2009, large deflection analysis of FG plates under pressure loads was performed using first and third-order shear deformation theories by Khabbaz *et al.* (2009). Furthermore, high-order tetrahedral finite element was employed for geometrically nonlinear analysis of structures composed of FG rubber-like materials Pascon and Coda (2013). A review on the subject of different theories and solution methods of laminated and sandwich plate and shells was performed by Caliri Jr. *et al.* (2016). Besides, Tiar *et al.* (2016) presented a Total Lagrangian formulation for geometrically nonlinear analysis of 2-D fiber-reinforced composite structures. The formulation allowed modeling of both long and short fibers embedded in matrix phase. A four-node quadrilateral element and a 2-node truss element were utilized to model the matrix and the fibers, respectively. In another research, Liu and Paavola (2016) proposed an analytical sensitivity analysis for sandwich shells. Both classical and first-order shear deformation theories were taken into account. Moreover, Liang (2017) developed an extended version of Kioster-Newton method to analyze the nonlinear buckling behavior of thick and thin composite plates. Timoshenko laminated beam theory was

used to eliminate the shear locking problem. In another article, the effects of different through the thickness approximation functions in conjunction with Carrera Unified Formulation for analysis of composite plate and shell structures were investigated by Carrera *et al.* (2016). A nine-node quadrilateral shell element with Mixed Interpolation of Torsorial Component method was used in their work. Furthermore, Coda *et al.* (2017) proposed an enhanced Zig-Zag theory for analyzing the laminated plates and shells. Their formulation behaved well for both displacements, and transverse stresses predictions.

Another research was dedicated to buckling analysis of laminated composite cylindrical shells using an analytical finite strip method by Khayat *et al.* (2016). Moreover, post-buckling analysis of laminated composite shells subjected to shear loads by Jung *et al.* (2016). Alankaya and Oktem (2016) implemented the static analysis of laminated sandwich shallow shells. They used third order shear deformation theory. In addition, a 6-node triangular laminated element for geometrically nonlinear analysis of composite shells was presented by Rezaiee-Pajand and Arabi (2016). It should be added that Mixed Interpolation of Torsorial Component method was employed to prevent the membrane and shear locking phenomenon. Some new researches were developed for nonlinear analysis of FG structures, especially cylindrical / hyperbolic FG shells and thick cross-ply panels by Chaudhuri *et al.* (Chaudhuri *et al.* 2014, 2015, Chaudhuri and Oktem 2015).

In this paper, an iso-parametric six-node element hereafter named as TRI6 shell element is formulated for geometric nonlinear analysis of FG shells. The main scope of this paper is to predict the nonlinear behavior of FG shells by utilizing the equivalent single layer theories of laminates. It is worth mentioning that the direct formulation of FGMs is also included. In addition, the ceramic volume fraction is represented as a power function of the thickness coordinate. The nonlinear procedure is based on the Total Lagrangian formulation, including large displacements and rotations. Some popular benchmarks are analyzed. Findings declare the accuracy and correctness of the proposed methods.

2. Finite element description

In this section, the incremental displacement for the TRI6 shell element is presented. The Total Lagrangian formulation is employed for large displacements and rotations. This element has three corner and three mid-side nodes. In the following equations, a superscript t is used to show load step and configuration. It is assumed that the director vector of nodes stays straight and unstretched during deformation. The geometry configuration of the TRI6 shell element, at the time t , is shown in Fig. 1.

The relation obtained for the geometry of the TRI6 shell element is as follows

$$\begin{Bmatrix} {}^t x \\ {}^t y \\ {}^t z \end{Bmatrix} = \sum_{j=1}^6 N_j(\xi, \eta) \begin{Bmatrix} {}^t x_j \\ {}^t y_j \\ {}^t z_j \end{Bmatrix} + \frac{\zeta}{2} \sum_{j=1}^6 {}^t N_j(\xi, \eta) \begin{Bmatrix} {}^t V_{n1}^j \\ {}^t V_{n2}^j \\ {}^t V_{n3}^j \end{Bmatrix} \quad (1)$$

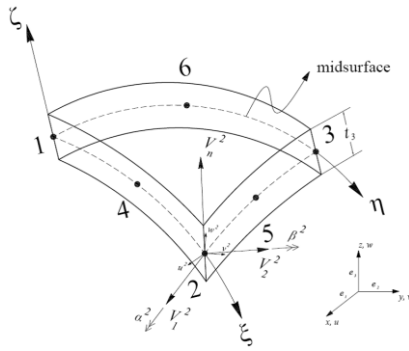


Fig. 1 Geometry of TRI6 shell element

In this relation, the two-dimensional interpolation functions of the six-node iso-parametric element are defined as $N_j(\xi, \eta)$. In addition, ξ, η and ζ are the local coordinates. Furthermore, the position vector components of node j at the global Cartesian coordinate system is shown by x_j, y_j and z_j . Furthermore, t_j define the thickness and the components of director vector of node j are presented by V_{n1}^j, V_{n2}^j and V_{n3}^j . The following equation expresses the incremental displacement in the element configuration at the time t to $t+\Delta t$

$$\begin{Bmatrix} u \\ v \\ w \end{Bmatrix} = \sum_{j=1}^6 N_j(\xi, \eta) \begin{Bmatrix} u_j \\ v_j \\ w_j \end{Bmatrix} + \frac{\zeta}{2} \sum_{j=1}^6 t_j N_j(\xi, \eta) \begin{Bmatrix} t+\Delta t V_{n1}^j \\ t+\Delta t V_{n2}^j \\ t+\Delta t V_{n3}^j \end{Bmatrix} - \begin{Bmatrix} tV_{n1}^j \\ tV_{n2}^j \\ tV_{n3}^j \end{Bmatrix} \quad (2)$$

where u_j, v_j and w_j are the incremental displacement at the node j . To determine the orientation of director vector at the time $t+\Delta t$ from time t , the finite rotation theory is utilized. Based on this scheme, two unit vectors of $\{tV_1^j\}$ and $\{tV_2^j\}$ are defined as follows

$$\begin{Bmatrix} tV_1^j \\ tV_2^j \end{Bmatrix} = \begin{Bmatrix} tV_{11}^j \\ tV_{12}^j \\ tV_{13}^j \end{Bmatrix} = \begin{Bmatrix} \frac{e_{22} tV_{n3}^j - e_{23} tV_{n2}^j}{\Delta} \\ -\frac{e_{21} tV_{n3}^j - e_{23} tV_{n1}^j}{\Delta} \\ \frac{e_{21} tV_{n2}^j - e_{22} tV_{n1}^j}{\Delta} \end{Bmatrix}, \quad (3)$$

$$\begin{Bmatrix} tV_{21}^j \\ tV_{22}^j \\ tV_{23}^j \end{Bmatrix} = \begin{Bmatrix} \frac{tV_{n2}^j tV_{13}^j - tV_{n3}^j tV_{12}^j}{\Delta} \\ -\frac{tV_{n1}^j tV_{13}^j - tV_{n3}^j tV_{11}^j}{\Delta} \\ \frac{tV_{n1}^j tV_{12}^j - tV_{n2}^j tV_{11}^j}{\Delta} \end{Bmatrix},$$

$$\Delta = \sqrt{\left((e_{22}^t V_{n3}^j - e_{23}^t V_{n2}^j)^2 + (e_{21}^t V_{n3}^j - e_{23}^t V_{n1}^j)^2 + (e_{21}^t V_{n2}^j - e_{22}^t V_{n1}^j)^2 \right)} \quad (3)$$

$$\Delta = \sqrt{\left((tV_{n2}^j tV_{13}^j - tV_{n3}^j tV_{12}^j)^2 + (tV_{n1}^j tV_{13}^j - tV_{n3}^j tV_{11}^j)^2 + (tV_{n1}^j tV_{12}^j - tV_{n2}^j tV_{11}^j)^2 \right)}$$

where e_{ij} are the components of unit vectors of Cartesian coordinates. After some simplification, the incremental displacement can be written in the subsequent form

$$\begin{Bmatrix} u \\ v \\ w \end{Bmatrix} = \sum_{j=1}^6 N_j(\xi, \eta) \begin{Bmatrix} u_j \\ v_j \\ w_j \end{Bmatrix} + \frac{\zeta}{2} \sum_{j=1}^6 t_j N_j(\xi, \eta) \left[-\alpha_j \begin{Bmatrix} tV_{21}^j \\ tV_{22}^j \\ tV_{23}^j \end{Bmatrix} + \beta_j \begin{Bmatrix} tV_{11}^j \\ tV_{12}^j \\ tV_{13}^j \end{Bmatrix} \right] - \frac{\zeta}{4} \sum_{j=1}^6 t_j N_j(\xi, \eta) \begin{Bmatrix} tV_{n1}^j \\ tV_{n2}^j \\ tV_{n3}^j \end{Bmatrix} \quad (4)$$

here α_j and β_j are the rotation degrees of freedom at node j . It is worth mentioning that these rotations are about $\{tV_1^j\}$ and $\{tV_2^j\}$ vectors.

3. Strain formulation

The metric vectors used in this formulation are given as

$$\begin{Bmatrix} t\bar{g}_1 \\ t\bar{g}_2 \\ t\bar{g}_3 \end{Bmatrix} = \begin{Bmatrix} \left\{ \frac{\partial^t x}{\partial \xi}, \frac{\partial^t y}{\partial \xi}, \frac{\partial^t z}{\partial \xi} \right\}^T \\ \left\{ \frac{\partial^t x}{\partial \eta}, \frac{\partial^t y}{\partial \eta}, \frac{\partial^t z}{\partial \eta} \right\}^T \\ \left\{ \frac{\partial^t x}{\partial \zeta}, \frac{\partial^t y}{\partial \zeta}, \frac{\partial^t z}{\partial \zeta} \right\}^T \end{Bmatrix} \quad (5)$$

In addition, the strain vector, at the time t with respect to time 0, has the following shape

$$\begin{Bmatrix} t\epsilon_{11} \\ t\epsilon_{22} \\ t\epsilon_{12} \\ t\epsilon_{13} \\ t\epsilon_{23} \end{Bmatrix} = \frac{1}{2} \begin{Bmatrix} t\bar{g}_1 \cdot t\bar{g}_1 - 0\bar{g}_1 \cdot 0\bar{g}_1 \\ t\bar{g}_2 \cdot t\bar{g}_2 - 0\bar{g}_2 \cdot 0\bar{g}_2 \\ t\bar{g}_1 \cdot t\bar{g}_2 - 0\bar{g}_1 \cdot 0\bar{g}_2 \\ t\bar{g}_1 \cdot t\bar{g}_3 - 0\bar{g}_1 \cdot 0\bar{g}_3 \\ t\bar{g}_2 \cdot t\bar{g}_3 - 0\bar{g}_2 \cdot 0\bar{g}_3 \end{Bmatrix} \quad (6)$$

Therefore, the subsequent incremental strains can be found as below

$$\begin{Bmatrix} 0\varepsilon_{11} \\ 0\varepsilon_{22} \\ 0\varepsilon_{12} \\ 0\varepsilon_{13} \\ 0\varepsilon_{23} \end{Bmatrix} = \frac{1}{2} \begin{Bmatrix} 2(u_{,1}^t g_{11} + v_{,1}^t g_{12} + w_{,1}^t g_{13}) \\ 2(u_{,2}^t g_{21} + v_{,2}^t g_{22} + w_{,2}^t g_{23}) \\ (u_{,1}^t g_{21} + u_{,2}^t g_{11}) + (v_{,1}^t g_{22} + v_{,2}^t g_{12}) + (w_{,1}^t g_{23} + w_{,2}^t g_{13}) \\ (u_{,1}^t g_{31} + u_{,3}^t g_{11}) + (v_{,1}^t g_{32} + v_{,3}^t g_{12}) + (w_{,1}^t g_{33} + w_{,3}^t g_{13}) \\ (u_{,2}^t g_{31} + u_{,3}^t g_{21}) + (v_{,2}^t g_{32} + v_{,3}^t g_{22}) + (w_{,2}^t g_{33} + w_{,3}^t g_{23}) \end{Bmatrix} \quad (7)$$

$$+ \frac{1}{2} \begin{Bmatrix} (u_{,1}u_{,1} + v_{,1}v_{,1} + w_{,1}w_{,1}) \\ (u_{,2}u_{,2} + v_{,2}v_{,2} + w_{,2}w_{,2}) \\ (u_{,1}u_{,2} + v_{,1}v_{,2} + w_{,1}w_{,2}) \\ (u_{,1}u_{,3} + v_{,1}v_{,3} + w_{,1}w_{,3}) \\ (u_{,2}u_{,3} + v_{,2}v_{,3} + w_{,2}w_{,3}) \end{Bmatrix}$$

Eq. (7) can be divided into linear and nonlinear parts, which are given in the short form as

$$\{0\varepsilon\} = \{0\varepsilon_l\} + \{0\varepsilon_{nl}\} \quad (8)$$

where subscript l and nl denote the linear and nonlinear strain, respectively. In order to alleviate the shear and membrane locking, the following interpolation functions are used for in-plane strains

$$\begin{aligned} \varepsilon_{\xi\xi} &= a_1 + b_1\xi + c_1\eta \\ \varepsilon_{\eta\eta} &= a_2 + b_2\xi + c_2\eta \\ \varepsilon_{q\eta} &= a_3 + b_3\xi + c_3(1 - \xi - \eta) \end{aligned} \quad (9)$$

For the transverse shear strains, the subsequent interpolation functions are used

$$\begin{aligned} \varepsilon_{\xi\zeta} &= a_1 + b_1\xi + c_1\eta + d_1\xi\eta + f_1\eta^2 \\ \varepsilon_{\eta\zeta} &= a_2 + b_2\xi + c_2\eta + d_2\xi\eta + f_2\xi^2 \end{aligned} \quad (10)$$

where the unknown coefficients in Eqs. (9) and (10) have been presented in Lee and Bathe (2004). Based on the Eq. (9), the in-plane shear strain is obtained as follow

$$\varepsilon_{\xi\eta} = \frac{1}{2}(\varepsilon_{\xi\xi} + \varepsilon_{\eta\eta}) - \varepsilon_{q\eta} \quad (11)$$

4. FGM and equivalent single layer formulation

In order to model the FG shells, a laminate composed of several laminas that are perfectly bonded together is assumed. Three models, including two, four and six layers are declared in Fig. 2. Each layer is considered to be

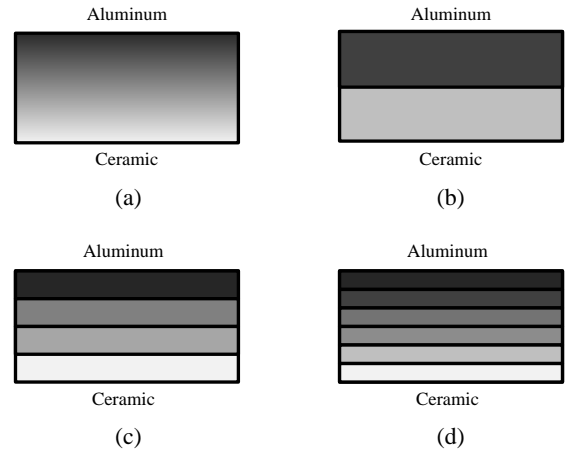


Fig. 2 The model of FG shell and the equivalent single layers: (a) The main model of FG shell; (b) The equivalent two layers; (c) The equivalent four layers; (d) The equivalent six layers

isotropic. To find the material properties of each layer, the thickness coordinates of each lamina middle surface (z_k) is substituted in the following volume fraction relations

$$\begin{aligned} f_c &= \left(\frac{z_k}{t} + \frac{1}{2}\right)^n \\ f_m &= 1 - f_c \end{aligned} \quad (12)$$

where f_c and f_m are the ceramic and metal volume fraction in power law. The exponent of volume fraction is defined by n . After that, the material properties of each layer are determined by utilizing the rule of mixture.

$$E(z_k) = E_c f_c + E_m f_m \quad (13)$$

The components of the reduced plane stress constitutive matrix of each layer are written in terms of the engineering constants as

$$[D_k] = \frac{E(z_k)}{1 - \nu^2} \begin{bmatrix} 1 & \nu & 0 & 0 & 0 \\ \nu & 1 & 0 & 0 & 0 \\ & & \frac{1}{2}(1 - \nu) & 0 & 0 \\ \text{Sym.} & & & \frac{1}{2}(1 - \nu) & 0 \\ & & & & \frac{1}{2}(1 - \nu) \end{bmatrix}_{5 \times 5} \quad (14)$$

In order to transfer the material matrix from local to global coordinates, the base vectors, which have been expressed in Eq. (5), can be used.

5. Equilibrium equations

The stiffness matrix of element is formulated in global coordinates system in which the metric vectors are utilized for transformation. Based on the principle of virtual work, the expression of the linearized equation of motion is given

below

$$\int_{q_V} [D] \{ {}_0\varepsilon_l \} \delta \{ {}_0\varepsilon_l \}^0 dV + \int_{q_V} \{ {}_0^t S \} \delta \{ {}_0\varepsilon_{nl} \}^0 dV = \{ {}^{t+\Delta t} R \} - \int_{q_V} \{ {}_0^t S \} \delta \{ {}_0\varepsilon_l \}^0 dV \quad (15)$$

where the $\{ {}_0^t S \}$ is the second Piola-Kirchhoff stress vector. Moreover, the linear and nonlinear components of the Green-Lagrange strain tensor are denoted by $\{ {}_0\varepsilon_l \}$ and $\{ {}_0\varepsilon_{nl} \}$, respectively. By substituting the incremental stress-strain relations in the equilibrium equation, the linear and nonlinear stiffness matrix can be obtained, as follows

$$\left(\left[{}_0^t K_l \right] + \left[{}_0^t K_{nl} \right] \right) \{ d \} = \{ {}^{t+\Delta t} R \} - \{ {}_0^t F \} \quad (16)$$

In this relation, $\{ d \}$ is the vector of nodal degrees of freedom. Furthermore, $\left[{}_0^t K_l \right]$ and $\left[{}_0^t K_{nl} \right]$ are the linear and nonlinear stiffness matrices. On the other hand, the external and internal forces are defined by $\{ {}^{t+\Delta t} R \}$ and $\{ {}_0^t F \}$, respectively.

6. Numerical study

To show the correctness of the proposed formulation for modeling the FG shells, several popular benchmark structural shells are solved by employing proposed TRI6 shell element. The results of these geometric nonlinear analyses are reported and compared by the solutions proposed in pervious investigations. In addition, a comparison will be performed to show the minimum layers, which can be used to simulate the FG shells for obtaining the accurate and correct responses. Note that the nonlinear solution approach used in numerical examples is the Generalized Displacement Control method.

It is worth mentioning that the following assumptions are utilized for all the examples. First, the module of

elasticity is changed FG along the shell thickness. Herein, seven different values, including 0.0, 0.2, 0.5, 1.0, 5.0, 10.0 and 100.0 are considered for the amount of exponent n in power function of elastic modulus. Second, the materials used here are Zirconia and Aluminum as ceramic and metal for the bottom and top surfaces Arciniega and Reddy (2007b). Furthermore, the elastic modulus of each layer in equivalent layer modeling is determined based on the main power function and assumed to be constant. Their values are calculated for different amounts of the exponent n and reported in Table 1. Moreover, Poisson’s ratio is assumed to be constant in this model and equal to 0.3.

It should be mentioned that at the first example, a comparison between the results obtained by the proposed equivalent layer formulation, including 2, 4 and 6 layers and the reference solutions are presented. Other examples will declare the responses of FG formulation and that of equivalent single layer theory.

6.1 Shallow panel

In this example, a shallow panel with two different amount of thickness is studied. The model of the shell

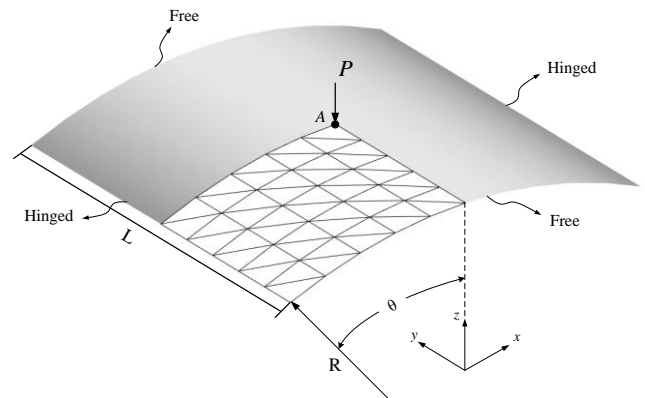


Fig. 3 Shallow panel under middle point load

Table 1 Elastic modulus of each layer for various values of exponent n and number of layers

Number of layer	Centre of layer position	n					
		0	0.2	0.5	1.0	5.0	100
2	3.175	151000	146471.1	140148.1	130750.0	89221.7	70000
	-3.175	151000	131386.5	110500.0	90250.0	70079.1	70000
4	4.763	151000	148865.4	145768.6	140875.0	111545.6	70000
	1.588	151000	143732.9	134036.1	120625.0	77724.8	70000
	-1.588	151000	136571.9	119602.2	100375.0	70600.7	70000
	-4.763	151000	123440.1	98637.8	80125.0	70002.5	70000
6	5.292	151000	149602.6	147551.6	144250.0	122425.5	70000
	3.175	151000	146471.1	140148.1	130750.0	89221.7	70000
	1.058	151000	142722.4	131864.8	117250.0	75471.0	70000
	-1.058	151000	137989.6	122285.3	103750.0	71017.3	70000
	-3.175	151000	131386.5	110500.0	90250.0	70079.1	70000
	-5.292	151000	119277.5	93382.7	76750.0	70000.3	70000



Fig. 4 Deformed configuration of shallow panel at the end of loading steps

structure and its mesh pattern is illustrated in Fig. 3. Here, the performance of the TRI6 shell element will be investigated for large deformation analysis of FG shells by using a different number of layers, which are used throughout the thickness. This structure is analyzed by two different amount of thickness, equal to 12.7 mm and 6.35 mm. The corresponding maximum load, which is applied in the center of the shallow panel, is equal to 200,000 N and 100,000 N, respectively.

The geometry characteristics of this structure are given below.

$$L = 508 \text{ mm} \quad R = 2540 \text{ mm} \quad \theta = 0.1 \text{ (rad)}$$

It should be added that the equilibrium paths for FG shallow panels with the different amount of power index n were previously obtained by Arciniega and Reddy (2007b). Due to symmetrical geometry of structure, only a quarter of the panel is modeled. The mesh of $(5 \times 5 \times 2)$ is used for finite element discretization. The results are obtained for two different amount of thickness, including 12.7 mm and 6.35 mm. Different volume fraction exponents n are investigated from fully metal to fully ceramic. Fig. 4 shows the last deformed configuration of the shallow panel.

The deflection at center point of the shallow panel is depicted in Fig. 5 for the different number of layers (2, 4 and 6 layers). In addition, the responses are compared with the results obtained by Arciniega and Reddy (2007b).

The agreement between the results of present study and the reference solution demonstrates the accuracy of authors' scheme for nonlinear analysis of FG shells using equivalent single layer theory. The outputs are presented for three numbers of layers, including 2, 4 and 6. The obtain results declare that the 6-layer modeling results almost matches well with the reference responses.

According to the given results in Fig. 5, it is observed that the deflections, which are achieved for various numbers of layers, are almost the same within the range of power index n smaller than 1.0. However, they show more differences when the factor n becomes greater than 1.0.

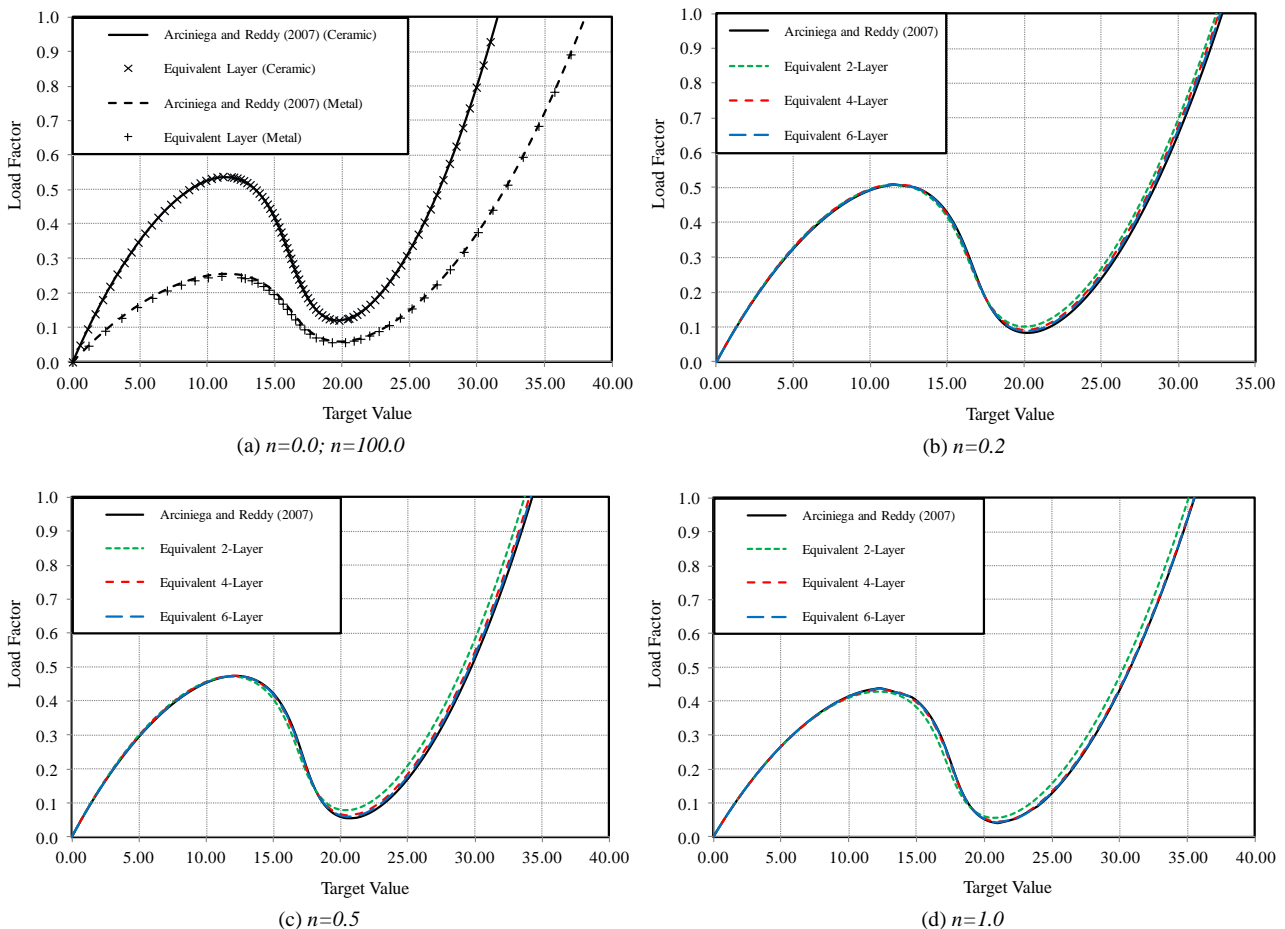


Fig. 5 The equilibrium path of 12.7-thickness shallow panel at the point A for the different number of layers and values of power index n

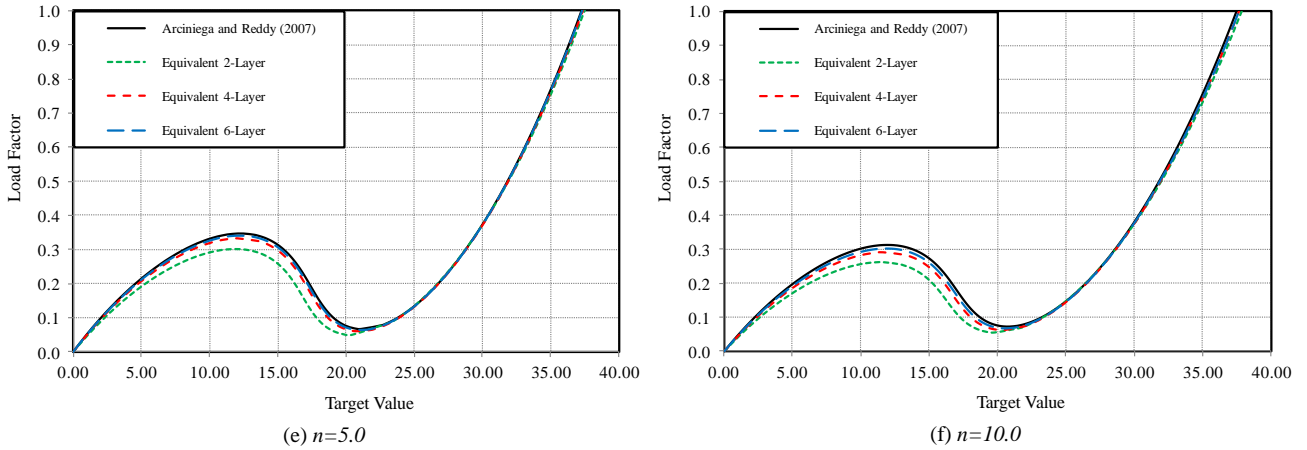


Fig. 5 Continued

It should be mentioned that in the case of using fully ceramic or metal, as the material properties are invariable along the thickness of the shell, the number of layers are not effective on the responses. Hence, an equivalent layer can be utilized for modeling the related shell structure. This fact is illustrated in Fig. 5(a).

Based on the results obtained from Fig. 5, equivalent 6-layer model is employed for analyzing the 6.35-thickness shallow panel. The load-deflection curves at the center point of structure are presented in Fig. 6 for different

values of power exponent n . The comparison of the present results with the related FG model solutions shows the ability of the present formulation in predicting the snap-through and snap-back behaviors. However, some minor drift is observed between the responses of the two formulations at the end part of the equilibrium path.

To compare the obtained responses with the reference solutions, the results are presented for the thickness of 12.7 mm shallow panel in Table 2. The results are provided for three states of FGM power exponent (n) including, 0.0, 1.0

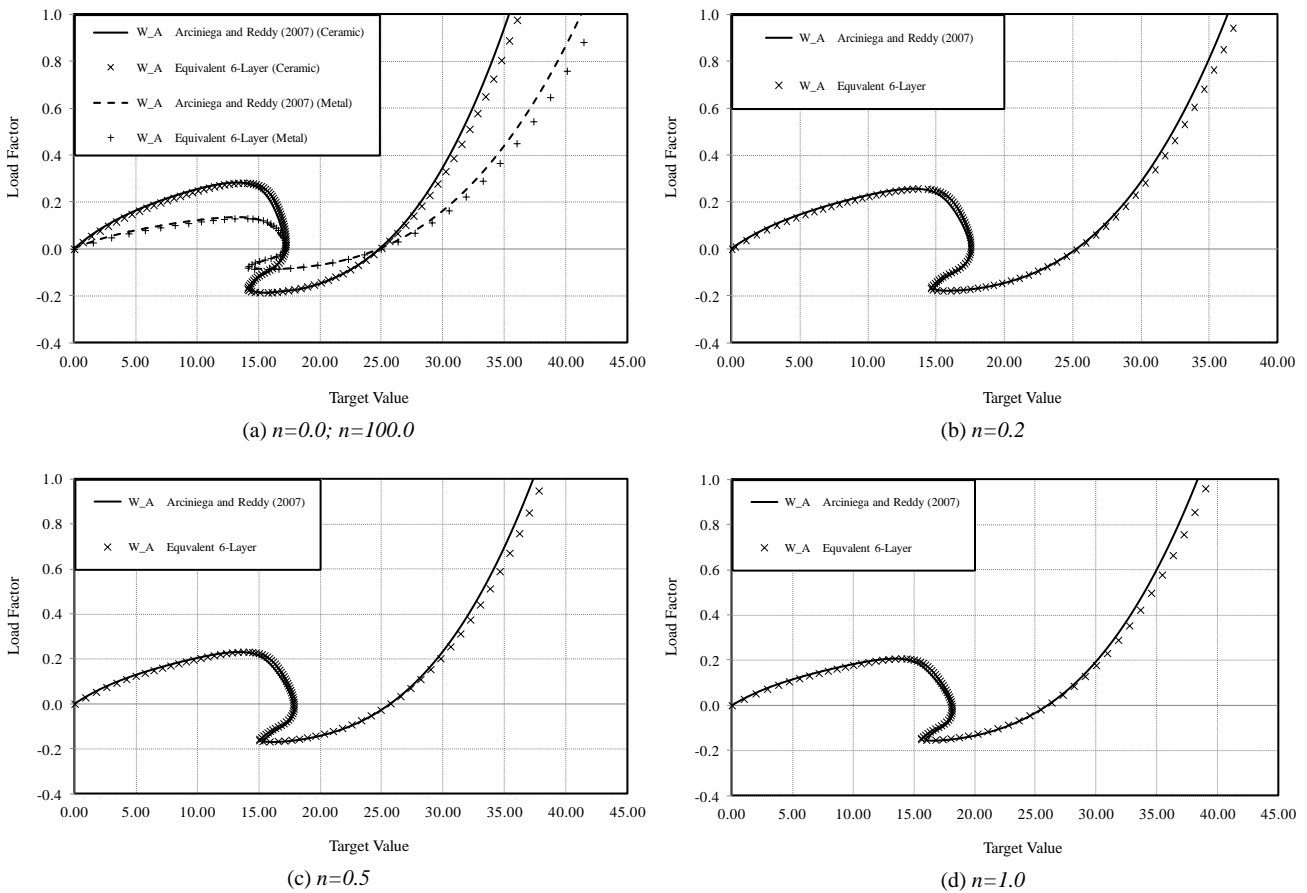


Fig. 6 Load vs. deflection of 6.35-thickness shallow panel at point A for different values of the power exponent n

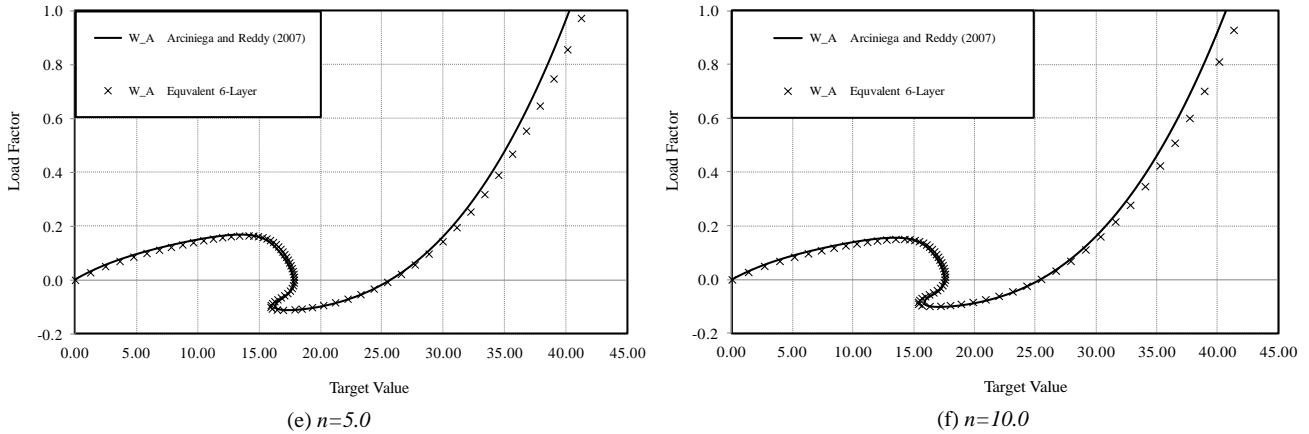


Fig. 6 Continued

Table 2 The results of vertical displacement of 12.7 mm-thickness shallow panel at point A

P/P_{max}	$n = 0.0$		$n = 1.0$		$n = 100.0$		P/P_{max}	Present formulation	Arciniega and Reddy (2007)
	Present formulation	Arciniega and Reddy (2007)	Present formulation	Arciniega and Reddy (2007)	Present formulation	Arciniega and Reddy (2007)			
0.0484	0.55466	0.55468	0.0480	0.74586	0.74549	0.0468	1.16326	1.16443	
0.2546	3.30579	3.30586	0.1755	3.00201	3.00044	0.1602	4.69993	4.70463	
0.4191	6.33557	6.33567	0.2997	5.82024	5.81692	0.2555	11.9289	11.9408	
0.5379	11.1493	11.1495	0.4385	12.4657	12.4657	0.2015	15.0270	15.0571	
0.4055	15.1441	15.1445	0.3047	16.7420	16.7253	0.1280	16.6045	16.6378	
0.2546	16.6156	16.6160	0.1104	18.6664	18.6645	0.0593	20.0740	20.1345	
0.1206	19.7553	19.7568	0.0416	21.1337	21.0914	0.1550	25.1226	25.1982	
0.3074	24.7651	24.7566	0.2047	26.6007	26.5741	0.2650	27.8807	28.0490	
0.4048	26.0777	26.0687	0.4005	29.5875	29.4988	0.4318	30.9469	31.1651	
0.6249	28.4340	28.4243	0.6982	32.8891	32.7904	0.7616	35.4064	35.6560	
0.9991	31.4959	31.4855	1.0225	35.7077	35.5292	0.9800	37.7614	38.0659	

and 100. This comparison shows the good agreement between the obtained outputs, and the responses reported by Arciniega and Reddy (2007b). It should be mentioned that the related reference reported the results in the equilibrium paths form. Therefore, the authors digitized the reference paths, and the values are reported in several steps of loading and compared with the obtained responses.

6.2 Clamped semi-cylindrical shell

Another popular benchmark problem is a semi-cylindrical shell which is shown in Fig. 7. The shell is clamped at two ends, and the two sides of semi-cylindrical shell are assumed to be roller supported. The maximum point load which is incrementally applied at the center of the shell structure is equal to 100,000. The geometric properties of structure used in this problem are considered as follows

$$L = 304.8 \text{ mm} \quad R = 101.6 \text{ mm} \quad t = 3.0 \text{ mm}$$

As it is seen in Fig. 7, one-half of the structure is modeled. To achieve the high accuracy, the number of TRI6

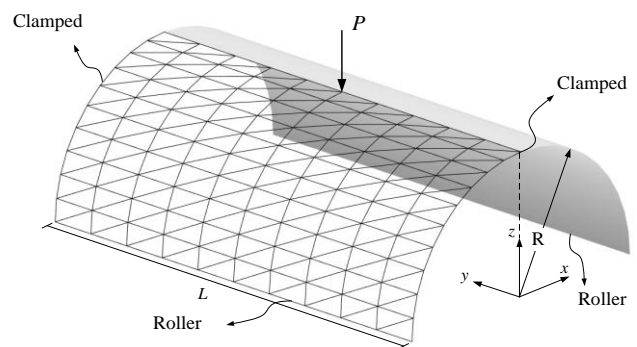


Fig. 7 Semi-cylindrical shell under the middle point load

shell element used for this problem is equal to 200. The deformed shape of structure at the end of loading is illustrated in Fig. 8.

Two cases of modeling are considered in this example. At first, the semi-cylindrical panel is analyzed using FG formulation. Next, the same structure is investigated considering the equivalent 6-layer model. Note that the analyses are performed for different values of FGM power

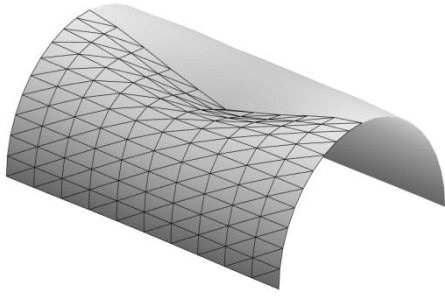
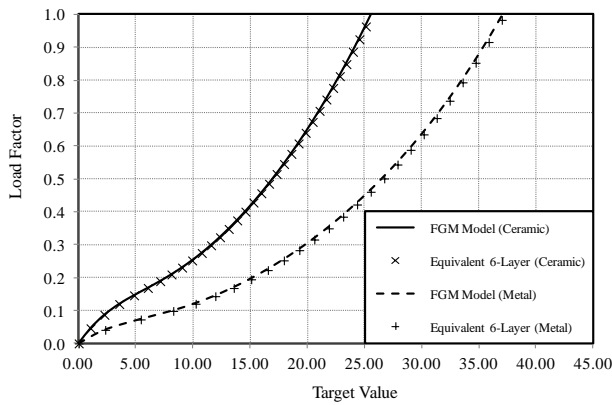


Fig. 8 Deformed shape of clamped semi-cylindrical shell at the final load step

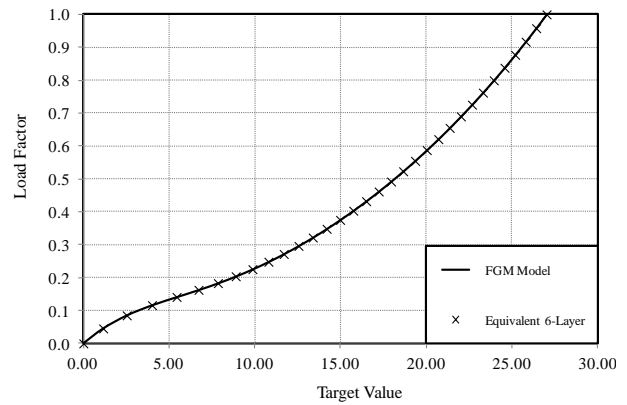
exponent n . The equilibrium path of semi-cylindrical shell is obtained for the center point and is depicted in Fig. 9. The obtained results for FG model and related equivalent layer are quite similar to each other. This shows the accuracy and capability of proposed equivalent formulation for modeling FG shell structures.

6.3 Hyperbolic shell

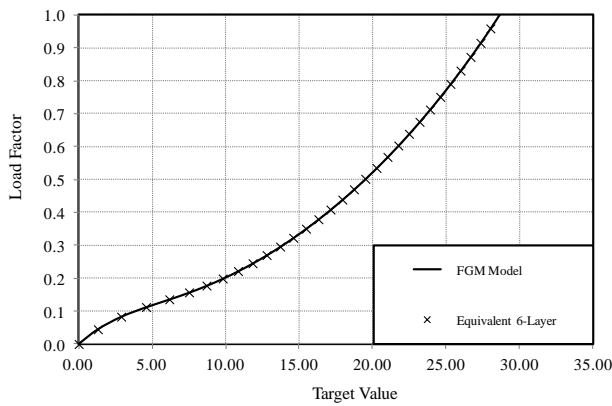
A FG hyperbolic shell, under two inward and two outward point loads, is investigated here. Fig. 10 shows the configuration of this problem. The geometric properties of



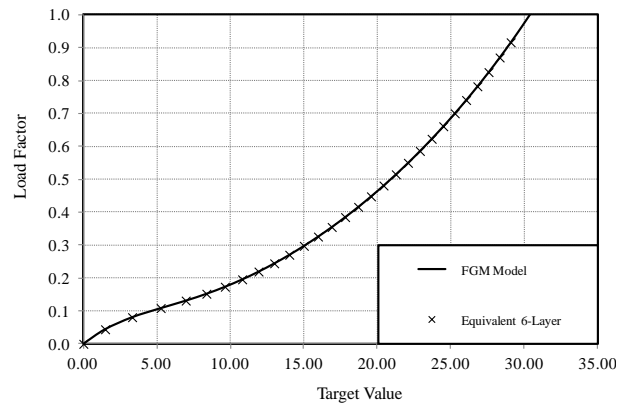
(a) $n=0.0$; $n=100.0$



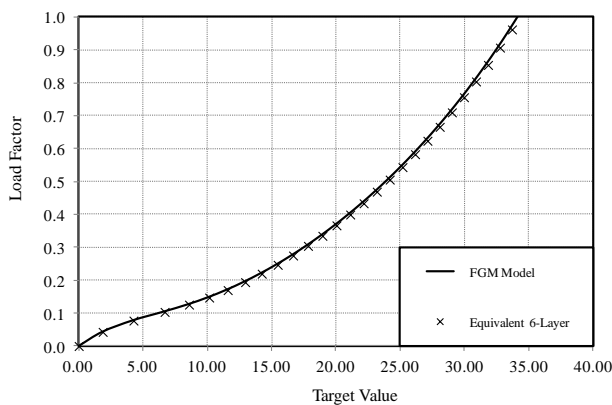
(b) $n=0.2$



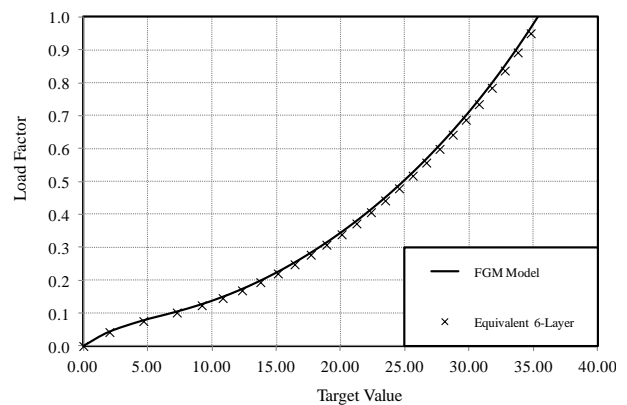
(c) $n=0.5$



(d) $n=1.0$



(e) $n=5.0$



(f) $n=10.0$

Fig. 9 Load-displacement curves of semi-cylindrical shell for different values of FGM power exponent n

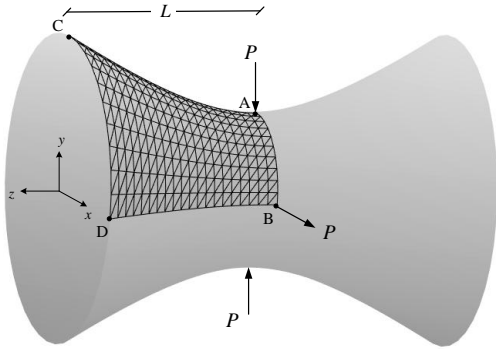


Fig. 10 Hyperbolic shell under two inward and two outward point loads

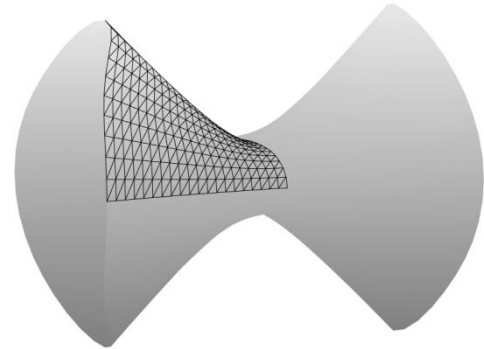
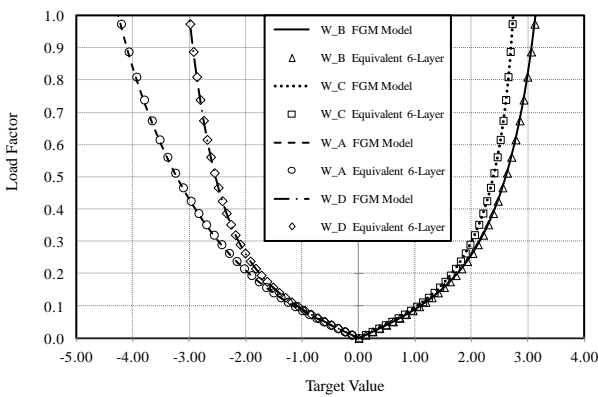
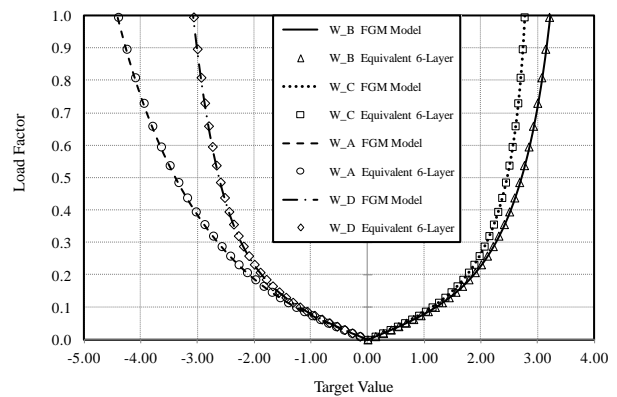


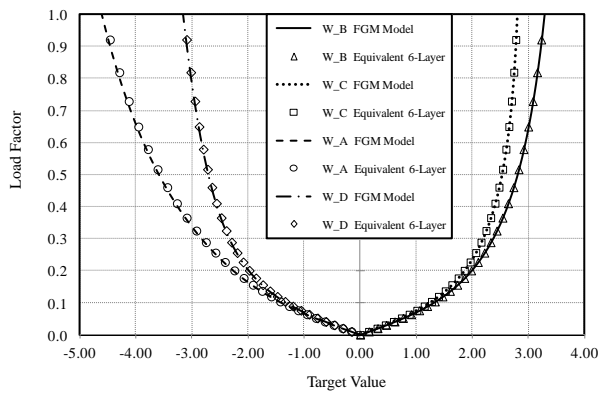
Fig. 11 Deformed shaped of hyperbolic shell at the end of analysis



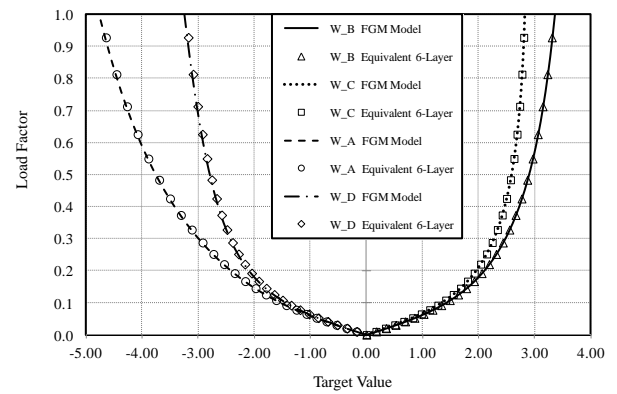
(a) $n=0.0$ (Ceramic)



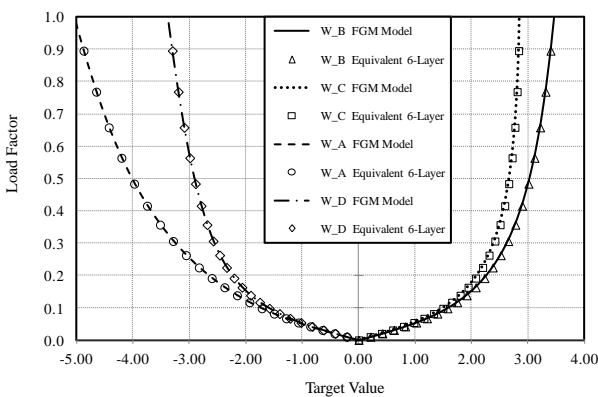
(b) $n=0.2$



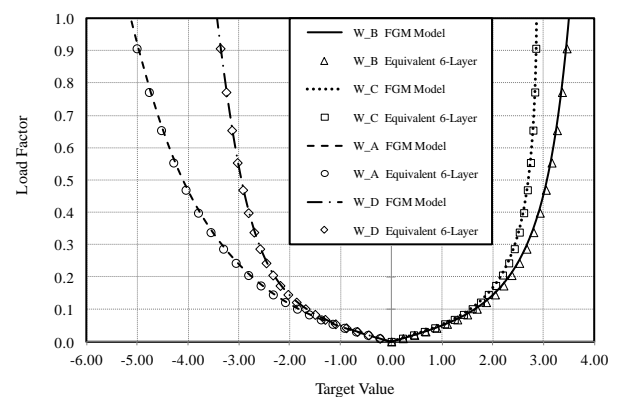
(c) $n=0.5$



(d) $n=1.0$

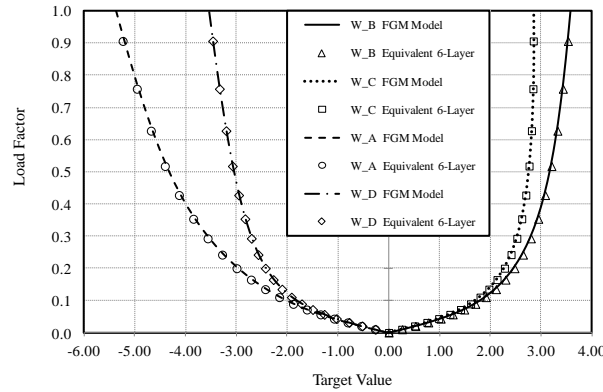


(e) $n=5.0$



(f) $n=10.0$

Fig. 12 Nonlinear displacements of points A, B, C and D versus point loads for various power law index n



(g) $n=100.0$ (Metal)

Fig. 12 Continued

this structure are found below.

$$L = 20.0 \quad R_1 = 7.5 \quad R_2 = 15.0 \quad t = 0.04$$

where R_1 and R_2 are the minimum and maximum radius of hyperbolic shell at the middle and end sections, respectively. The units of all parameters are mm.

Moreover, the maximum loads applied at the middle of the shell are equal to 4. The number of TRI6 shell elements employed in this model is assumed to be 400. Based on Fig. 10 and owing to symmetry, only one-eighth of the shell is used for analyzing. In addition, the last deformed configuration of hyperbolic shell at the end of analysis is declared in Fig. 11.

For different points: A, B, C and D, the load-displacement curves obtained from the FG and equivalent 6-layer models are provided in Fig. 12. The analysis is carried out for different values of power index n . The achieved responses clearly demonstrated that the obtained displacements of the FGM formulation and equivalent 6-layer modeling are in good agreement. These show the accuracy and high applicability of the present formulation in modeling arbitrary shell geometries even with high geometric nonlinearity behaviors.

6.4 Cylindrical shell subjected to pull-out forces

This example is dedicated to solve a 0.094-thickness cylindrical shell structure under the pull-out forces. The elastic modulus and Poisson's ratio of homogenous material are respectively equal to 10.5×10^6 and 0.3125. Fig. 13 depicts the structural geometric properties. It is worth mentioning that the two ends of the cylinder are free. Due to symmetry, an octant of the cylinder is discretized by using $10 \times 10 \times 2$ triangular shell elements.

This problem was also investigated by Sze *et al.* (2004). To show the locking phenomena in the nonlinear analysis of shell structures, especially thin shells, two states of formulation are considered in this study. In case one, the structure is analyzed using the mixed interpolation of strain formulation. On the other hand, the problem is also solved based on the iso-parametric formulation without any additional strain interpolation. The results of both states are presented in Table 3 and compared with the reference solution of Sze *et al.* (2004). According to the obtained responses, it can be concluded that the additional mixed interpolation, which is considered in the proposed formulation, can avoid locking phenomena in the nonlinear analysis of shell structures, especially thin shells.

Table 3 The results of tip displacement of point A in a pull-out cylindrical shell

P/P_{\max}	Sze <i>et al.</i> (2004)	Present formulation	Without interpolation	P/P_{\max}	Sze <i>et al.</i> (2004)	Present formulation	Without interpolation
0.000	0.0000	0.00000	0.00000	0.500	2.4730	2.46805	2.34455
0.025	0.8190	0.81982	0.78335	0.525	2.5430	2.53791	2.36541
0.050	1.2600	1.26012	1.20370	0.550	2.5770	2.61147	2.38456
0.075	1.5270	1.52837	1.45677	0.600	2.6180	2.72141	2.45237
0.100	1.7070	1.70888	1.63445	0.650	2.6480	2.75259	2.48225
0.150	1.9360	1.93832	1.85263	0.700	2.6720	2.77754	2.51388
0.200	2.0790	2.08110	1.99499	0.750	2.6920	2.79833	2.54700
0.250	2.1800	2.18436	2.08118	0.800	2.7100	2.81704	2.55158
0.300	2.2570	2.25993	2.14622	0.850	2.7260	2.83368	2.57759
0.350	2.3210	2.32565	2.21197	0.900	2.7410	2.84927	2.59177
0.400	2.3760	2.37909	2.25626	0.950	2.7550	2.86382	2.62497
0.450	2.4250	2.42791	2.35072	1.000	2.7680	2.87733	2.63735

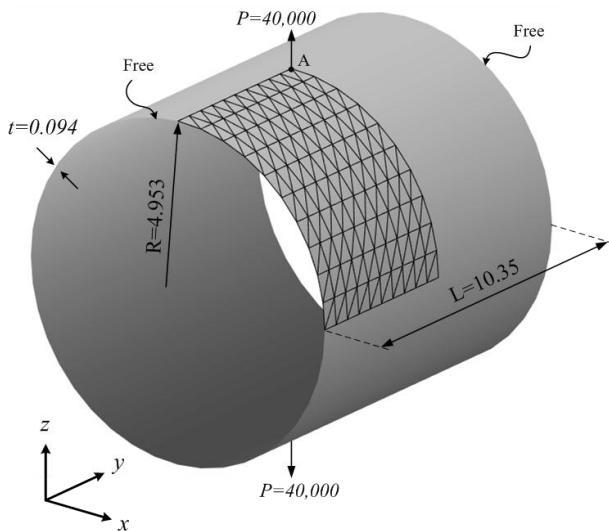


Fig. 13 The free-ends cylindrical shell under pull-out forces

7. Conclusions

In this study, the geometrically nonlinear analysis of FG shells based on the equivalent single layer theory, and direct FG formulation was performed. At first, the minimum number of layers, which were required for proper modeling of the FG shells, was evaluated. In this process, three cases were employed with a different number of layers, including two, four and six. Findings declared that the accurate, and near exact solutions can be concluded by using six layers throughout the thickness of the shell. Therefore, the other examples were investigated by using six layers. Moreover, the FG formulation was also included. It should be added that the authors employed a locking free six-node triangular element entitled TRI6 shell element utilizing the MITC approach. Furthermore, first-order shear deformation theory was used in the present formulation. In addition, the volume fraction of FGM was formulated as a power function with exponent of n . Finally, the results were obtained for the different values of n . It was observed that the differences between the results obtained from FGM model and the responses of equivalent layers scheme increases by enhancing the value of power exponent n . In other words, it seems that the equivalent layers model is more appropriate for lower values of the power exponent. Another interesting contribution of this article was analyzing the different type of curved shells, especially hyperbolic shell structures. The good agreement of the obtained results for this type of shell structures with complex geometry can prove the high capability of the proposed shell element. The hyperbolic shell analyzed in this research is very thin, and the obtained equilibrium paths showed the locking free of the new shell element.

Based on the geometric properties of the other examples, it can be concluded that the element is applicable for analyzing the thin and moderately thick shell structures. Some other popular benchmarks of shell structures were also analyzed based on authors' scheme. The outputs illustrated the validity and high accuracy of the present formulations. Finally, another benchmark problem was

solved in two cases of with and without strain interpolation. It was found that the proposed mixed interpolation of strains can alleviate the occurrence of locking phenomena, especially in thin shell structures.

Funding: This study was not funded by any company.

Conflict of Interest: The authors declare that they have no conflict of interest.

References

- Ahmad, S., Irons, B. and Zienkiewicz, O.C. (1970), "Analysis of thick and thin shell structures by curved finite elements", *Int. J. Numer. Method. Eng.*, **2**(3), 419-451.
- Alankaya, V. and Oktem, A.S. (2016), "Static analysis of laminated and sandwich composite doubly-curved shallow shells", *Steel Compos. Struct., Int. J.*, **20**(5), 1043-1066.
- Arciniega, R.A. and Reddy, J.N. (2007a), "Large deformation analysis of functionally graded shells", *Int. J. Solids Struct.*, **44**(6), 2036-2052.
- Arciniega, R.A. and Reddy, J.N. (2007b), "Tensor-based finite element formulation for geometrically nonlinear analysis of shell structures", *Comput. Method. Appl. Mech. Eng.*, **196**(4-6), 1048-1073.
- Barbosa, J.A.T. and Ferreira, A.J.M. (2009), "Geometrically nonlinear analysis of functionally graded plates and shells", *Mech. Adv. Mater. Struct.*, **17**(1), 40-48.
- Bathe, K.J. (1982), *Finite Element Procedures in Engineering Analysis*, Prentice-Hall, Englewood Cliffs.
- Beheshti, A. and Ramezani, S. (2015), "Nonlinear finite element analysis of functionally graded structures by enhanced assumed strain shell elements", *Appl. Math. Model.*, **39**(13), 3690-3703.
- Caliri Jr., M.F., Ferreira, A.J.M. and Tita, V. (2016), "A review on plate and shell theories for laminated and sandwich structures highlighting the Finite Element Method", *Compos. Struct.*, **156**, 63-77.
- Carrera, E., Cinefra, M., Li, G. and Kulikov, G.M. (2016), "MITC9 shell finite elements with miscellaneous through-the-thickness functions for the analysis of laminated structures", *Compos. Struct.*, **154**, 360-373.
- Chaudhuri, R.A. and Oktem, A.S. (2015), "Analysis of simply-supported saddle-shaped symmetric cross-ply panels with no surface-parallel boundary constraints", *AIAA J.*, **54**(2), 782-788.
- Chaudhuri, R.A., Oktem, A.S. and Guedes Soares, C. (2014), "Levy-type boundary Fourier analysis of thick clamped hyperbolic-paraboloidal cross-ply panels", *AIAA J.*, **53**(1), 140-149.
- Chaudhuri, R.A., Oktem, A.S. and Guedes Soares, C. (2015), "Levy-type boundary Fourier analysis of thick cross-ply panels with negative Gaussian curvature", *AIAA J.*, **53**(9), 2492-2503.
- Coda, H.B., Paccola, R.R. and Carrazedo, R. (2017), "Zig-Zag effect without degrees of freedom in linear and non linear analysis of laminated plates and shells", *Compos. Struct.*, **161**, 32-50.
- Dvorkin, E.N. and Bathe, K.J. (1984), "A continuum mechanics based four-node shell element for general nonlinear analysis", *Eng. Comput.*, **1**(1), 77-88.
- Hughes, T.J.R. and Liu, W.K. (1981a), "Nonlinear finite element analysis of shells-part II. two-dimensional shells", *Comput. Method. Appl. Mech. Eng.*, **27**(2), 167-181.
- Hughes, T.J.R. and Liu, W.K. (1981b), "Nonlinear finite element analysis of shells: Part I. three-dimensional shells", *Comput. Method. Appl. Mech. Eng.*, **26**(3), 331-362.
- Jung, W.-Y., Han, S.-C., Lee, W.-H. and Park, W.-T. (2016), "Postbuckling analysis of laminated composite shells under

- shear loads”, *Steel Compos. Struct., Int. J.*, **21**(2), 373-394.
- Kaci, A., Belakhdar, K., Tounsi, A. and Bedia, E.A.A. (2014), “Nonlinear cylindrical bending analysis of E-FGM plates with variable thickness”, *Steel Compos. Struct., Int. J.*, **16**(4), 339-356.
- Kapania, R.K. (1989), “A Review on the Analysis of Laminated Shells”, *J. Press. Vessel Tech.*, **111**(2), 88-96.
- Khabbaz, R.S., Manshadi, B.D. and Abedian, A. (2009), “Nonlinear analysis of FGM plates under pressure loads using the higher-order shear deformation theories”, *Compos. Struct.*, **89**(3), 333-344.
- Khayat, M., Poorveis, D. and Moradi, S. (2016), “Buckling analysis of laminated composite cylindrical shell subjected to lateral displacement-dependent pressure using semi-analytical finite strip method”, *Steel Compos. Struct., Int. J.*, **22**(2), 301-321.
- Khayat, M., Poorveis, D. and Moradi, S. (2017), “Buckling analysis of functionally graded truncated conical shells under external displacement-dependent pressure”, *Compos. Struct., Int. J.*, **23**(1), 1-16.
- Kim, K.-D., Lomboy, G.R. and Han, S.-C. (2008), “Geometrically non-linear analysis of functionally graded material (FGM) plates and shells using a four-node quasi-conforming shell element”, *J. Compos. Mater.*, **42**(5), 485-511.
- Lee, P.S. and Bathe, K.J. (2004), “Development of MITC isotropic triangular shell finite elements”, *Comput. Struct.*, **82**(11-12), 945-962.
- Levyakov, S.V. and Kuznetsov, V.V. (2011), “Application of triangular element invariants for geometrically nonlinear analysis of functionally graded shells”, *Comput. Mech.*, **48**(4), 499-513.
- Liang, K. (2017), “Koiter–Newton analysis of thick and thin laminated composite plates using a robust shell element”, *Compos. Struct.*, **161**, 530-539.
- Liu, Q. and Paavola, J. (2016), “General analytical sensitivity analysis of composite laminated plates and shells for classical and first-order shear deformation theories”, *Compos. Struct.*, **183**, 21-34.
- Liu, W.K., Law, E.S., Lam, D. and Belytschko, T. (1986), “Resultant-stress degenerated-shell element”, *Comput. Methods Appl. Mech. Eng.*, **55**(3), 259-300.
- Crisfield, M. (1986), *Finite Elements on Solution Procedures for Structural Analysis, (I) Linear Analysis*, Pineridge Press, Swansea, UK.
- Masoodi, A.R. and Arabi, E. (2018), “Geometrically nonlinear thermomechanical analysis of shell-like structures”, *J. Thermal Stress.*, **41**(1), 37-53.
- Park, K.C. and Stanley, G.M. (1986), “A curved C0 shell element based on assumed natural-coordinate strains”, *J. Appl. Mech.*, **53**(2), 278-290.
- Pascon, J.P. and Coda, H.B. (2013), “High-order tetrahedral finite elements applied to large deformation analysis of functionally graded rubber-like materials”, *Appl. Math. Model.*, **37**(20), 8757-8775.
- Reddy, J.N. and Arciniega, R.A. (2004), “Shear Deformation Plate and Shell Theories: From Stavsky to Present”, *Mech. Adv. Mater. Struct.*, **11**(6), 535-582.
- Rezaiee-Pajand, M. and Arabi, E. (2016), “A curved triangular element for nonlinear analysis of laminated shells”, *Compos. Struct.*, **153**, 538-548.
- Rezaiee-Pajand, M. and Masoodi, A.R. (2018), “Exact natural frequencies and buckling load of functionally graded material tapered beam-columns considering semi-rigid connections”, *J. Vib. Control*, **24**(9), 1787-1808.
- Rezaiee-Pajand, M., Arabi, E. and Masoodi, A.R. (2018a), “A triangular shell element for geometrically nonlinear analysis”, *Acta Mechanica*, **229**(1), 323-342.
- Rezaiee-Pajand, M., Masoodi, A.R. and Mokhtari, M. (2018b), “Static analysis of functionally graded non-prismatic sandwich beams”, *Adv. Comput. Des.*, **3**(2), 165-190.
- Sze, K.Y., Liu, X.H. and Lo, S.H. (2004), “Popular benchmark problems for geometric nonlinear analysis of shells”, *Finite Elem. Anal. Des.*, **40**(11), 1551-1569.
- Thai, H.-T. and Kim, S.-E. (2015), “A review of theories for the modeling and analysis of functionally graded plates and shells”, *Compos. Struct.*, **128**(15), 70-86.
- Tiar, A., Zouari, W., Kebir, H. and Ayad, R. (2016), “A nonlinear finite element formulation for large deflection analysis of 2D composite structures”, *Compos. Struct.*, **153**, 262-270.
- Uysal, M.U. (2016), “Buckling behaviours of functionally graded polymeric thin-walled hemispherical shells”, *Steel Compos. Struct., Int. J.*, **21**(4), 849-862.
- Wetherhold, R.C., Seelman, S. and Wang, J. (1996), “The use of functionally graded materials to eliminate or control thermal deformation”, *Compos. Sci. Technol.*, **56**(9), 1099-1104.
- Woo, J. and Meguid, S.A. (2001), “Nonlinear analysis of functionally graded plates and shallow shells”, *Int. J. Solids Struct.*, **38**(42), 7409-7421.
- Zhao, X. and Liew, K.M. (2009), “Geometrically nonlinear analysis of functionally graded shells”, *Int. J. Mech. Sci.*, **51**(2), 131-144.

CC